Lattice dynamics of SiC polytypes within the bond-charge model

M. Hofmann, A. Zywietz, K. Karch, and F. Bechstedt
Friedrich-Schiller-Universität, Institut für Festkörpertheorie und Theoretische Optik, Max-Wien-Platz 1, 07743 Jena, Germany
(Received 7 April 1994)

We present a phenomenological approach to the lattice-dynamical properties of various SiC polytypes. A generalized bond-charge model is applied to the cubic and hexagonal polytypes $3C$, $6H$, $4H$, and $2H$. The long-range microscopic electric field of ions and bond charges is fully taken into account via an Ewald technique. The short-range elastic interactions are described by bending and stretching forces between ions and bond changes. The force constants and effective charges are fit to phonon frequencies known from Raman and luminescence measurements. The reliability of the model is tested not only for the frequencies but also for the eigenvectors by comparison with results of *ab initio* calculations for $3C$- and $2H$-SiC. We show that the anisotropy in the uniaxial hexagonal polytypes is mainly due to the nonanalyticity of the Coulomb forces. The corresponding frequency splittings are related to slight changes of the bond charges in dependence on the bond orientation. Differences in the elastic forces parallel and nonparallel to the hexagonal axis are only necessary to stabilize the zone-boundary phonons. The trends of the resulting frequencies and density of states are discussed versus the percentage hexagonality. Consequences of the different phonon dispersions for the elastic properties of $3C$, $6H$, $4H$, and $2H$ polytypes are considered. We speculate about possible mechanisms of polytype stabilization by the lattice vibrations.

I. INTRODUCTION

Silicon carbide (SiC) is a semiconductor which combines very interesting physical and chemical properties. The extreme thermal and chemical stability together with the large electron saturation velocity and mobility make it a very prominent candidate for electronic devices able to work under hostile environments (such as high temperature, corrosive atmosphere, or irradiation) with excellent high-power and high-frequency performance. The large band gaps have made possible the application of SiC crystals in blue-light-emitting diodes. The different applicative possibilities are supported by the high thermal conductivity as well as mechanical stability. From the physical point of view SiC has exciting structural properties. It is the only IV-IV compound forming stable and, moreover, long-ranged ordered structures, the so-called polytypes.[1] The low stacking fault energy causes that more than 100 different polytypes crystallizing in the cubic (C), hexagonal (H), and rhombohedral (R) system have been observed.[2,3] They differ by the stacking arrangement of the N Si-C bilayers in the cubic [111] direction within a unit cell indicated by the notation $3C$, NH, or NR.

The understanding of the lattice-vibrational properties is important for an explanation of various interesting properties of SiC, among them mechanical, thermal, and structural ones. The phenomenon of polytypism can be related also to phonons. Phonons may stabilize the polytypism via different contributions to the free energy.[4] Furthermore, it has been demonstrated how the long-ranged interatomic interactions determining the polytypes arise from the phonons.[5] *Ab initio* calculations of the phonon spectra are rare.[6–10] They are moreover restricted to the zinc-blende $3C$ structure[6–8] with one exception concerning the wurtzite $2H$-SiC.[9] The same holds for the phenomenological models. The normal modes of lattice vibrations in cubic SiC have been investigated on the basis of rigid-ion models (RIM's),[11–16] a deformation dipole model (DDM),[17] and valence overlap shell model (VOSM).[7] Within the RIM approaches only short-range force constants[12,13,15,17] or short-range central and noncentral interactions as well as long-range Coulomb interactions among ions of appropriate effective charges have been considered.[11,14,16]

In contrast to theory many experimental studies of the vibrational properties of various polytypes exist. Raman scattering has been extensively used to study the phonons in $3C$, $2H$, $4H$, $6H$, $15R$, and $21R$.[8,17–20] Besides, many infrared absorption and reflectivity measurements have been reported for $3C$, $6H$, $10H$, and $15R$.[21–24] However, only few luminescence studies are known for $3C$, $2H$, $6H$, and $15R$, in which vibrational frequencies have been derived from phonon replica.[25,26]

In this paper we develop a phenomenological model for the description of the lattice dynamics of cubic $3C$-SiC and hexagonal $6H$-, $4H$-, and $2H$-SiC. This approach does not only give correct frequencies and their trends with the hexagonality but also reasonable eigenvectors, i.e., atomic displacement fields. For reasons discussed below we choose the adiabatic bond-charge model (BCM).[27] In Sec. II the elastic forces and electric charges are related to different polytypes. The free parameters are fitted to frequencies known from different experiments. In Sec. III the results for the phonon band structures and the densities of states are discussed versus the percentage hexagonality. We study the reasons for the

anisotropy, in particular the angular dispersion and the splitting of the modes in the zone center. Consequences of the differences in the lattice dynamics are discussed for structural and thermal properties of the polytypes. Finally, in Sec. IV a brief summary is given.

II. LATTICE DYNAMICAL MODEL AND POLYTYPE STRUCTURE

A. Bond-charge model

Phonon frequency dispersion relations present a useful test for a reasonable description of the lattice dynamics of crystals. However, it has been pointed out dynamical matrix uniquely.[28] Only the combination of eigenvalues and eigenvectors does this. Indeed, different models can predict very similar frequencies but quite different eigenvectors.[17,29] This holds especially for the longitudinal modes, as clearly shown for the [111] direction in silicon.[29] Among various lattice-dynamical approaches, as e.g., the valence-force-field model (VFFM),[30] the BCM, and the partial-density model (PDM),[31] only the BCM correctly describes the behavior of the longitudinal mode along the Λ direction apart from *ab initio* calculations.[10]

Starting point of the lattice-dynamical model is the introduction of bond charges (BC's) according to Phillips[32] and Martin.[33] The three types of bonding in the system—metal-like, covalent, and ionic bonding—are represented by different short-range and long-range interactions as schematically indicated in Fig. 1. The massless BC's carry the effective (screened) charge $-Z_{\mathrm{BC}}$ in a near midbond position. These electrons are transferred from the atoms. Because of the tetrahedrally coordination they carry the ion charge $2Z_{\mathrm{BC}}$. The partially ionic bonding is modeled by displacing the BC from the midbond position between Si and C by a relative shift p $(0 \leq p \leq 1)$ toward the carbon atom. The limiting cases $p = 0$ and $p = 1$ represent completely covalent or ionic bonding. The relative shift is thus a measure of the ionicity or heteropolarity of the bond. For the zinc-blende structure we choose $p = \frac{1}{3}$ according to the maximum position of the total valence electron density derived within an *ab initio* density-functional calculation.[9,34] This value is somewhat larger as in the case of III-V compounds, where the bonds between anions and cations are shared in a 3:5 ratio instead of 2:3.[27,35] It reflects the remarkable differences in the covalent radii as well as electronegativities of Si and C.[36] The total electrostatic energy of the arising system of point charges is calculated by means of the Ewald method.[37] The bond lengths are kept fixed according to the experimental lattice constants a (in the cubic case) or c and a (in the hexagonal cases).[38] The small atomic relaxations[39] and the variation of p around $\frac{1}{3}$ (Ref. 34) are neglected for the hexagonal polytypes. The BC Z_{BC} is used as a free parameter, and varied in accordance with the bond orientation.

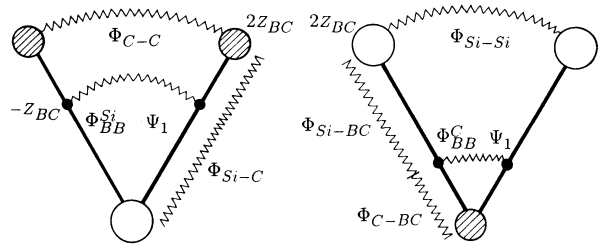

FIG. 1. Schematic representation of the interactions within the adiabatic bond-charge model. The indicated force constants and charges are defined within the text.

Besides the Coulomb forces at least three types of short-range elastic interactions are taken into account (cf. Fig. 1). The metal-like bonding behavior in the system is represented by a nearest-neighbor two-body force with a potential $\Phi_{\mathrm{Si\text{-}C}}$ between the Si and C ions. Similar central forces are assumed between a BC and a neighboring ion with potentials $\Phi_{\mathrm{Si\text{-}BC}}$ and $\Phi_{\mathrm{C\text{-}BC}}$. They describe effects of the covalent bonding. Furthermore bond-bending forces are taken into account. A bond-bond (BB) interaction of the Keating type is very important for the stability of the structures.[40] It gives rise to effective noncentral forces with potentials $\Phi^{\mathrm{Si}}_{\mathrm{BB}}$ and $\Phi^{\mathrm{C}}_{\mathrm{BB}}$ between the ions. An additional parameter, which is modifying the bond-bending forces and was necessary for a reasonable description of the lattice vibrations of diamond,[27] is not introduced. In order to take into account the strong bonding in the presence of carbon atoms we consider central forces between second-nearest-neighbor atoms as well as first- and second-nearest-neighbor bond charges with the potentials $\Phi_{\mathrm{Si\text{-}Si}}$, $\Phi_{\mathrm{C\text{-}C}}$, Ψ_1, and Ψ_2.

In the explicit fit each of the central forces is represented by two different force constants, a longitudinal and a transversal one. The longitudinal (transversal) force constant is related to the second (first) derivative of the corresponding potential, i.e., $\Phi''_{X\text{-}Y}$ or $\Psi''_{1/2}$ ($\Phi'_{X\text{-}Y}$ or $\Psi'_{1/2}$) with X,Y =Si,C,BC. On the other hand, the noncentral forces are characterized by only one parameter β_{Si} or β_{C} in dependence on the chemical nature of atom involved in the three-body interaction. Fortunately, all force constants are not linearly independent. For instance, the transversal constants follow from the equilibrium conditions. Consequently, in the zinc-blende case with two atoms per unit cell the adiabatic BCM employs ten disposable parameters, nine force constants and one BC. In the uniaxial systems $2H$, $4H$, and $6H$ under consideration the number of free parameters increases according to the different elastic interactions for bonds parallel or nonparallel to the c-axis as well as the anisotropy of the BC's.

B. Dynamical matrix and atomic geometry

Within the cubic zinc-blende structure of $3C$-SiC two atoms, Si and C, and four BC's belong to a unit cell. Labeling the six particles by $\kappa = 1$–6 the corresponding

positions are described by the vectors

$$\begin{aligned}
\mathbf{r}_1 &= (0,0,0),\\
\mathbf{r}_2 &= \frac{a}{4}(1,1,1),\\
\mathbf{r}_3 &= (1+p)\frac{a}{8}(1,1,1),\\
\mathbf{r}_4 &= (1+p)\frac{a}{8}(1,\bar{1},\bar{1}),\\
\mathbf{r}_5 &= (1+p)\frac{a}{8}(\bar{1},1,\bar{1}),\\
\mathbf{r}_6 &= (1+p)\frac{a}{8}(\bar{1},\bar{1},1).
\end{aligned} \tag{1}$$

When the position of the unit cell is described by a Bravais-lattice vector $\mathbf{R}_l$, the most important examples of the matrices of the short-range force constants $\hat{\Phi}_{\alpha\beta}\begin{pmatrix} l & l' \\ \kappa & \kappa' \end{pmatrix}(\alpha,\beta = x,y,z)$ are[27,41]

$$\begin{aligned}
\hat{\Phi}_{\alpha\beta}\begin{pmatrix} 0 & 0 \\ 1 & 2 \end{pmatrix} &= \frac{1}{3}\Phi''_{\text{Si-C}} + \frac{1}{3}\frac{\Phi'_{\text{Si-C}}}{d}(3\delta_{\alpha\beta}-1),\\
\hat{\Phi}_{\alpha\beta}\begin{pmatrix} 0 & 0 \\ 1 & 3 \end{pmatrix} &= \frac{1}{3}\Phi''_{\text{Si-BC}} + \frac{2}{3}\frac{\Phi'_{\text{Si-BC}}}{(1+p)d}(3\delta_{\alpha\beta}-1)\\
&\quad + \frac{1}{2}\beta_{\text{Si}}(2\delta_{\alpha\beta}-1),\\
\hat{\Phi}_{\alpha\beta}\begin{pmatrix} 0 & 0 \\ 3 & 6 \end{pmatrix} &= \frac{1}{4}\beta_{\text{Si}}(1-2\delta_{\alpha z})\\
&\quad + \frac{1}{2}\Psi''_1(1-\delta_{\alpha z})(1-\delta_{\beta z}),\\
\hat{\Phi}_{\alpha\beta}\begin{pmatrix} 0 & 1 \\ 1 & 1 \end{pmatrix} &= \frac{1}{2}\Phi''_{\text{Si-Si}}(1-\delta_{\alpha z})(1-\delta_{\beta z}),
\end{aligned} \tag{2}$$

with $d = \sqrt{3}a/4$ as the bond length. The other important interactions follow by an exchange of Si and C in the Eqs. (2).

The elastic energy of the lattice of ions and BC's follows immediately from the force-constant matrices of the type defined in Eqs. (2). However, because of the charged particles, the long-range Coulomb interactions have also to be taken into account. Their most important contribution is related to the Madelung energy $-\frac{1}{2}\alpha_M(2Z_{\text{BC}}e)^2/d$, where α_M denotes the Madelung constant of the considered structure. For the considered cubic case it amounts $\alpha_M = 5.044$. The variations of the total elastic energy with respect to the bond length d as well as to the position of the BC, defined by the heteropolarity parameter p, give the equilibrium conditions[27]

$$\{(1+p)\Phi'_{\text{Si-BC}} + (1-p)\Phi'_{\text{C-BC}}\} + 2\Phi'_{\text{Si-C}} + \frac{1}{2}\alpha_M(2Z_{\text{BC}}e/d)^2 = 0, \tag{3}$$

$$\frac{d_o}{2}\{\Phi'_{\text{Si-BC}} - \Phi'_{\text{C-BC}}\} - 2\frac{\partial\alpha_M}{\partial p}(Z_{\text{BC}}e)^2/d = 0.$$

The variation of the Madelung constant with the bond polarity is about $\partial\alpha_M/\partial p = 4.029$. A reasonable assumption is the vanishing of the first expression in parantheses.[27] It completes the system of equations for the three transversal force constants $\Phi'_{\text{Si-BC}}$, $\Phi'_{\text{C-BC}}$, and $\Phi'_{\text{Si-C}}$.

Besides the mentioned short-range interactions between ions, $\Phi_{\text{Si-C}}$, and ions and BC's, $\Phi_{\text{Si-BC}}$ and $\Phi_{\text{C-BC}}$, as well as the Keating potentials, $\Phi^{\text{Si}}_{\text{BB}}$ and $\Phi^{\text{C}}_{\text{BB}}$, we consider central forces between neighbored BC's (Ψ_1) and second-nearest-neighbor ions ($\Phi_{\text{Si-Si}}$ and $\Phi_{\text{C-C}}$) and BC's (Ψ_2). However, we assume that the accompanying transversal force constants are zero, i.e., $\Phi'_{\text{Si-Si}} = \Phi'_{\text{C-C}} = \Psi'_1 = \Psi'_2 = 0$. Indeed, a fit of these constants leads to negligible values in most cases. In addition the assumptions $\Psi''_1 = -\Psi''_2 = \frac{1}{2}(\beta_{\text{Si}} - \beta_{\text{C}})$ and $\Phi''_{\text{Si-Si}} = -\Phi''_{\text{C-C}}$ are introduced to reduce the number of free constants.[43] These assumptions correspond to those well-known from the covalent case, where the central forces between BC's and second-nearest-neighbor ions are completely neglected.[27,41]

Similar equations as given in Eqs. (2) and (3) are used in the hexagonal cases. There is an additional approximation, which however is nearly fulfilled. We neglect the small bond length and bond angle variations[39] by fixing the ideal ratio of the lattice constants $c/(Na) = (2/3)^{\frac{1}{2}}$. This assumption is supported by the small variations of the Madelung constant α_M and its derivative $\partial\alpha_M/\partial p$ (cf. Table III). The unit cells of the hexagonal polytypes $2H$, $4H$, and $6H$ are shown in Fig. 2 together with the hexagonal representation of the $3C$ zinc-blende structure. The positions of the atoms as well as the bond charges are indicated. This figure makes evident that in the uniaxial crystals, at least, two different types of bonds (and consequently bond charges) have to be distinguished. One sort of bonds is parallel to the c axis, whereas the other one forms angle with that axis of about 70.5°. Since all central forces act along a bond, we therefore introduce two different kinds of force constants of the ion-ion interactions labeled by $\|$ or $\perp$ in correspondence to the bond orientation. In the case of the BC's the situation is more complicated. The orientation dependence of the three-body forces and the second-nearest-neighbor interactions is less pronounced. Therefore, we apply the same constants Ψ''_1, Ψ''_2, β_{Si}, and β_{C} for all SiC polytypes. The anisotropy related to the BC's is assumed to be only caused by the long-range Coulomb interactions. Generally, we double the number of elastic force constants going from the cubic case to the hexagonal polytypes.

In the hexagonal polytypes the stacking sequence of Si-C bilayers in the cubic [111] direction in the form AB ($2H$), $ABCB$ ($4H$), or $ABCACB$ ($6H$) instead of ABC as known from the zinc blende induces automatically an anisotropy in the long-range electric field accompanying the atomic displacements. Thereby, the anisotropy is similar to case of artificial superlattices on the base of polar III-V compounds. However, the origins are different. Whereas in the case of semiconductor superlattices the different atomic masses are most important, the arrangement of ions and bond charges governs the effect in hexagonal SiC crystals. Nevertheless, we learn during the fit procedure that this natural electrical anisotropy has to be increased by splitting and changing the mag-

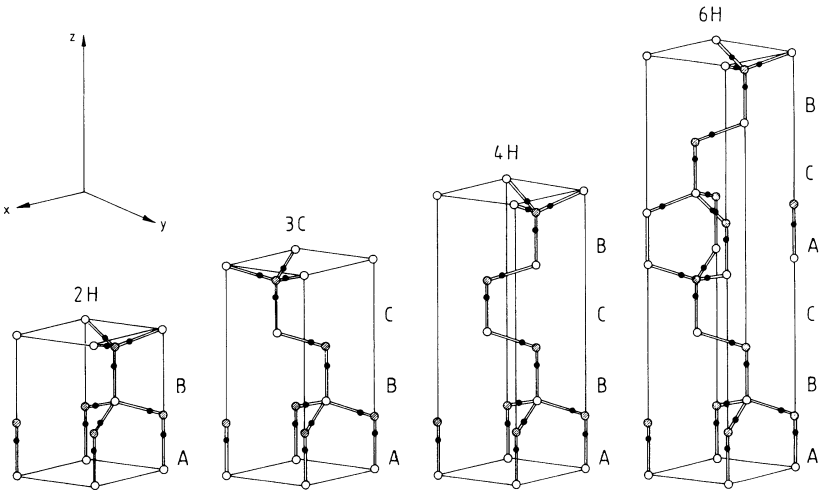

FIG. 2. Unit cells of the hexagonal SiC polytypes $2H$, $4H$, and $6H$. For completeness the $3C$ structure is also drawn in a hexagonal cell. Furthermore, the stacking sequences AB, ABC, $ABCB$, and $ABCACB$ are indicated. Si atoms are denoted by open circles, C atoms by hatched circles, and bond charges by dots.

nitude of the bond charges. In this way the remarkable angular dispersion and splittings of the zone-center optical phonons[17,18] can be explained in a satisfying manner. We differ between BC's $Z_{BC}^{||}$ and $Z_{BC}^{\perp}$ according to their positions on bonds parallel to the c axis or bonds forming an angle of about 70.5° with the c axis. An interesting consequence is the nonmonotoneous behavior of the Madelung constant as a function of the hexagonality (cf. Table III). It is due to the interplay of structure and BC splitting.

C. Force constants and hexagonality

The BC Z_{BC} and the force constants $\Phi''_{Si\text{-}C}$, $\Phi''_{Si\text{-}BC}$, $\Phi''_{C\text{-}BC}$, $\Phi''_{Si\text{-}Si}$ (or $\Phi''_{C\text{-}C}$), β_{Si}, and β_C are determined by a fit of the resulting eigenfrequencies to experimental frequencies from Raman scattering and luminescence measurements and are listed in Tables I and II. In the case of the ΓL direction in the Brillouin zone of $3C$-SiC we additionally use the phonon dispersion curves constructed by folding the phonon dispersion curves along the stacking direction of the different hexagonal and rhombohedral polytypes.[18] More strictly speaking, these dispersion curves are constructed from Raman data for $6H$, $4H$ (cf. Table I), $15R$, and $21R$ by identifying their weak modes with those with a certain finite wave vector in the $3C$ case.

In the fitting procedure (in particular for $3C$-SiC), explicitly a modified package UNISOFT (Ref. 42) of computer codes is applied. It contains the method of least squares to optimize the fit procedure. A starting point for the hexagonal polytypes are the BC and the force constants obtained for $3C$-SiC. However, in order to improve the fit near Γ and the high-symmetry point, which is related to the conduction-band minimum, we allow a splitting of Z_{BC} and the central-force constants according to the bond orientation. However, only one of the two constants with the subscript $||$ or $\perp$ is really changed between the polytypes. Thereby, we use the fact that the force constant $\Phi''_{Si\text{-}C}$ mainly influences the optical and LA branches, whereas the TA branches do practically not follow a variation of $\Phi''_{Si\text{-}C}$. The TA-like phonons are essentially fixed by the ion-BC potentials $\Phi_{Si\text{-}BC}$ and $\Phi_{C\text{-}BC}$ as well as the Coulomb forces. The Keating-like potentials Φ_{BB}^{Si} and Φ_{BB}^{C} displace the whole dispersion curves. Increasing (decreasing) the symmetric part of the force constants $\frac{1}{2}(\beta_{Si}+\beta_C)$ the curves shifts toward higher (lower) frequencies.

The results of the fitting procedure are listed in Table III. As in the case of diamond-structure materials[27] and zinc-blende III-V compounds[43] the first nearest-neighbor ion-ion and ion-BC interactions are the strongest ones. This holds especially for the constant $\Phi''_{C\text{-}BC}$, which is enhanced because of the small distance $(1-p)d/2$ of the two highly charged particles BC and C. The constants of the noncentral forces between the BC's are remarkably

TABLE I. Phonon frequencies (in cm^{-1}) of the strong and weak zone-center modes from Raman measurements (Refs. 18–20).

Mode		$3C$	$6H$	$4H$	$2H$
"strong"					
LO	A_{1l}	972.7	964	967	968.4
	E_{1l}		970	971	974.5
TO_1, TO_2	E_{1t}	796.2	797	797	799.1
	A_{1t}		788	782	769.8
"weak"					
axial o.	A_1		889	838	
planar o.	E_2		788	776	761.8
	E_1		777		
	E_1		769		
	E_2		769		
axial a.	A_1		508	610	
	A_1		504		
planar a.	E_2		262	266	263.6
	E_1		241	204	
	E_1		236	196	
	E_2		149		
	E_2		145		

TABLE II. Phonon frequencies (in cm^{-1}) of zone-boundary modes from luminesence measurements for hexagonal polytypes (Refs. 25, 26) and Raman studies for zinc-blende SiC (Ref. 19). The high-symmetry points L, X, M, and K in the two Brillouin zones are indicated.

Mode	$3C$ (L)	$3C$ (X)	$6H$ (M)	$2H$ (K)
LO	838	829	863	806.2
TO_1	766	761	771	737.3
TO_2			840	832.7
LA	610	640	430	498.6
TA_1	266	373	372, 293	498.6, 424.3
TA_2				

smaller as in other group IV and III-V materials. For β_{Si} we even find a negative value. Such a tendency is already observed for III-V compounds such as AlSb (Ref. 43) with large electronegativity differences. In any case it holds $\frac{1}{2}(\beta_{anion} - \beta_{cation}) > 0$ (Refs. 27, 35, 43) for the asymmetric part of the BC-ion-BC forces.

The BC Z_{BC}, which is an indirect measure of the strength of the covalent bonds in the system, is relatively large. It reaches larger values than in Si, Ge, and III-V semiconductors, but slightly smaller ones than in diamond. The force constants for the bond-stretching potentials of BC's and second-nearest-neighbor ions remain relatively small. Moreover, they carry different signs, what indicates a partial cancellation of their effects.

The trends with the percentage hexagonality h (Ref. 18) of the polytype, $h = 0$, 33, 50, and 100% for $3C$, $6H$, $4H$, or $2H$, respectively, according to the relative number of Si-C bilayers with hexagonal character, i.e., twisted bonds, are very interesting. The average value of the BC's in each bilayer, $(Z_{BC}^{||}+3Z_{BC}^{\perp})/4$, keeps the $3C$ value $Z_{BC} = 0.7984$. However, the difference $(Z_{BC}^{||} - Z_{BC}^{\perp})$ increases with h. Linear decreases with h are used for the force constants $\Phi''_{Si\text{-}C\perp}$, $\Phi''_{Si\text{-}BC||}$, whereas $\Phi''_{C\text{-}BC\perp}$ increases linearly. This behavior of the short-range interactions is probably related to a partial compensation of the effect due to the increase $(Z_{BC}^{||})$ or decrease $(Z_{BC}^{\perp})$ of BC's. There was no need for a change in the noncentral force constants as well as central force constants of the BC-BC interactions during the fitting procedure. We have only considered minor decreases of the second-nearest-neighbor interactions $\Phi''_{Si\text{-}Si||}$ and $\Phi''_{C\text{-}C\perp}$.

The discrepancies in the short-range elastic forces according to $||$ and $\perp$ as well as in the long-range electric forces related to the different BC's $Z_{BC}^{||}$ and $Z_{BC}^{\perp}$ give not only rise to an explanation of doublet splittings and anisotropy of the phonon modes. Rather, they may give some hints with respect to the thermodynamic stability of the polytypes. The varying forces lead to different interplanar interactions between the Si-C bilayers and consequently to small energy differences between the polytypes. The different strengths of the effective interplanar interactions between *cubic* and *hexagonal* bilayers in the various structures $3C$, $6H$, $4H$, and $2H$ may be a driving force for the stabilization of one polytype versus another one.

However, such a discussion exhibits at least two problems. First, there is no clear unique trend. The frequencies do not simply shift to higher (lower) values with rising hexagonality, what would stabilize the $2H$ ($3C$) structure at absolute zero of the temperature, whereas for higher temperatures the free energy of the lattice vibrations would tend to stabilize more the cubic polytype. Second, there remain difficulties in explaining the occurrence of particular long-period polytypes which may have N up to 100. Within the BCM the only origin for such a long-range driving force is the difference in the Coulomb interactions due to the varying splitting of BC's in $Z_{BC}^{||}$ and $Z_{BC}^{\perp}$ as well as the varying arrangement of ions and BC's.

TABLE III. Parameters of the bond-charge model used for the SiC polytypes. The screened BC's are in units of the electron charge, whereas the force constants are given in N/m. The Madelung constant and its derivative are dimensionless.

	$3C$	$6H$	$4H$	$2H$
$Z_{BC}^{||}$	0.79840	0.80623	0.81000	0.81500
$Z_{BC}^{\perp}$		0.79579	0.79453	0.79287
$\Phi''_{Si\text{-}C||}$	147.47	147.47	147.47	147.47
$\Phi''_{Si\text{-}C\perp}$		145.14	143.97	140.45
$\Phi''_{Si\text{-}BC||}$	245.82	244.15	243.32	240.82
$\Phi''_{Si\text{-}BC\perp}$		245.82	245.82	245.82
$\Phi''_{C\text{-}BC||}$	2660.80	2660.80	2660.80	2660.80
$\Phi''_{C\text{-}BC\perp}$		2734.00	2770.00	2880.00
ψ''_1	−40.17	−40.17	−40.17	−40.17
$\Phi''_{Si\text{-}Si||}$	29.12	29.12	29.12	29.12
$\Phi''_{Si\text{-}Si\perp}$		27.79	27.15	25.10
$\Phi''_{C\text{-}C||}$	−29.12	−28.53	−28.22	−27.32
$\Phi''_{C\text{-}C\perp}$		−29.12	−29.12	−29.12
ψ''_2	40.17	40.17	40.17	40.17
β_{Si}	−25.80	−25.80	−25.80	−25.80
β_C	54.55	54.55	54.55	54.55
α_M	5.044	5.115	5.067	5.039
$\frac{\partial \alpha_M}{\partial p}$	4.029	4.100	4.150	4.045

III. RESULTS

A. Eigenfrequencies

The phonon dispersion curves, obtained with Table III for $3C$-SiC along high-symmetry lines in the Brillouin zone of the fcc structure, are represented in Fig. 3. The experimental data given in Tables I and II (cf. Ref. 18) are indicated by circles and triangles. There is overall an excellent agreement between theoretical curves and available experimental data. This holds especially for LO, LA, and TA branches along ΓL. The dispersion of the TO branch is well described. However, its absolute position is slightly overestimated by theory. A good agreement is also observed for the X point. This is particularly satisfying because the TA(X) phonon mode can induce significant amounts of charge transfer between

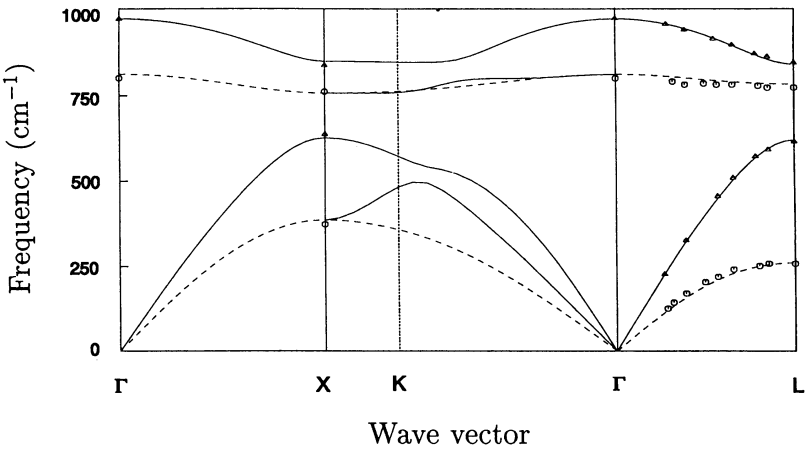

FIG. 3. Phonon dispersion curves for 3C-SiC. The experimental data from Tables I and II and Ref. 18 are represented as triangles and circles. Solid and dashed lines represent the calculated results of our BCM (cf. Table III). In the [100] and [111] directions the different lines indicate longitudinal (solid) and transversal (dashed) phonon polarization.

chemical bonds.[44] Unfortunately there are no experimental data for the mixed modes along the [110] direction. However, the most important features of the dispersion curves agree with those from *ab initio* calculations.[9]

In Fig. 4 we compare the phonon dispersion curves of the four polytypes 3C, 6H, 4H, and 2H under consideration versus high-symmetry directions in the hexagonal Brillouin zone. Obviously, the most important polytype influence is related to the reduced translational symmetry in the hexagonal [0001] direction. The number N of Si-C bilayers in the polytype determines the number of atoms per unit cell and, consequently, the number of phonon branches. The enlargement of the unit cell clearly causes the folding of the four branches along ΓL in the cubic 3C structure onto the shorter ΓA lines in the hexagonal Brillouin zone. However, the folding effect gives also rise to more branches in the other directions.

The agreement with the Raman data for the Γ point is excellent. Likewise, the frequency values for phonons from the zone boundary, which are obtained from luminescence measurements, are well reproduced. This holds especially considering the reduced accuracy of identifying the phonon modes from the replica of luminescence lines.

B. Anisotropy

The splitting at Γ between several optical branches belonging to different propagation directions ΓA or ΓK of the phonons is a characteristic feature for the hexagonal polytypes, in general for uniaxial crystals. The hexagonal polytypes NH-SiC ($N = 2, 4, 6$) belong to the space group C_{6v}^4 ($P6_3mc$). The phonon representation at the Γ point is reducible into representations A_1, E_1, E_2, and B_2. The A_1 and E_1 branches are both Raman active and infrared active. The E_2 branches are only Raman active, whereas the B_1 branches are inactive. The long-wavelength normal modes of a hexagonal polytype NH are $N(A_1 + B_1 + E_1 + E_2)$.

The optical modes are differently influenced by (i) the macroscopic electric field associated with the atomic displacements and (ii) the crystal anisotropy represented by the orientation-dependent short-range interactions.[45] There are strong modes which correspond to the zone-center LO and TO phonons of the zinc-blende structure. Moreover, weak modes exist which can be traced back to phonons with finite wave vector from the ΓL line in the cubic SiC. The Raman-active strong modes are remarkably influenced by the anisotropic macroscopic electric field. Therefore they depend on the angle Θ between the phonon propagation direction and the c axis. The strong modes have primarily longitudinal (l) or transverse (t) character because of the long-range electric field, but they have generally mixed symmetry of type $(A_1 + E_1)$. More in detail it holds for the strong modes LO, TO1, and TO2 (Ref. 45)

$$\begin{aligned}
&\omega_{\mathrm{LO}}^2(A_{1l} + E_{1l}) = \cos^2\Theta\omega^2(A_{1l}) + \sin^2\Theta\omega^2(E_{1l}),\\
&\omega_{\mathrm{TO1}}^2(E_{1t}) = \omega^2(E_{1t}),\\
&\omega_{\mathrm{TO2}}^2(A_{1t} + E_{1t}) = \sin^2\Theta\omega^2(A_{1t}) + \cos^2\Theta\omega^2(E_{1t}), \quad (4)
\end{aligned}$$

where for normal propagation the two transverse branches degenerate.

In Fig. 4 we have realized the cases $\Theta = 0°$ by the ΓA line and $\Theta = 90°$ by the ΓK line. The corresponding splittings between $\omega(A_{1l})$ and $\omega(E_{1l})$ as well as $\omega(A_{1t})$ and $\omega(E_{1t})$ can be plotted versus the hexagonality of the polytype. In accordance with our fitting procedure we observe a nearly linear behavior of the limiting frequencies with the hexagonality parameter h ($0 \le h \le 1$),

$$\begin{aligned}
\omega(E_{1l}) &= (979.0 - 3.1 \times h)\ \mathrm{cm}^{-1},\\
\omega(A_{1l}) &= (979.0 - 13.4 \times h)\ \mathrm{cm}^{-1},\\
\omega(E_{1t}) &= (795.7 + 3.8 \times h)\ \mathrm{cm}^{-1},\\
\omega(A_{1t}) &= (795.7 - 25.4 \times h)\ \mathrm{cm}^{-1}. \quad (5)
\end{aligned}$$

In optimizing the linear behavior with the hexagonality in Eqs. (5), the splittings of dispersion curves for ΓA and ΓK as well as the absolute positions of the TO-like phonons are carefully taken into account. That explains the lower agreement with experimental data[20] in the case of LO-like vibrations. We mention that the changes with the hexagonality can be essentially described by the small splittings and the variations of the BC's, $Z_{\mathrm{BC}}^{\parallel}$ and $Z_{\mathrm{BC}}^{\perp}$, with the polytype. In order to obtain the same effect by

the short-range elastic forces much stronger changes of the force constants have to be taken into account, which are not restricted to 1% as in the case of BC's.

The consequences of the electric-field-induced anisotropy can be also observed in integral quantities like the density of states. This can be seen from Fig. 5, where in addition to the total density for the zinc-blende structure the deviations from this one are plotted for $6H$, $4H$, and $2H$. Calculating the density of states the Dirac's δ function is Gaussian-broadened with a variance of 4 cm^{-1}. The Brillouin-zone integration is replaced by a **k**-space sampling involving for example 3696 mesh points in the $2H$ case.

The polytypism does only influence the density of states in the frequency region of the optical phonons. These changes increase with the percentage hexagonality. The sharp TO phonon peak in the $3C$ curve, essentially arising from the Γ point is split into two overlapping peaks, related strongly to E_{1t} or $(A_1 + E_1)_t$ phonons, in accordance with Eqs. (4). Smaller changes in the density distribution are found in the region of the LO phonon band of the $3C$ structure. With rising hexagonality this peak is broadened and its center of gravity is slightly shifted towards higher frequencies. The density of states near LO(Γ) of the zinc-blende is now distributed over a band limited by the two frequencies $\omega(A_{1l})$ and $\omega(E_{1l})$ [cf. Eqs. (4)]. On the other hand, changes in the spectral region of the former TA and LA branches remain small. They are mainly related to the tiny gaps appearing between different branches at Γ. At the new zone boundaries in the folded phonon band structure, i.e., at the A point, the branches are degenerated for symmetry reasons. Even in the case of vanishing gaps there can be

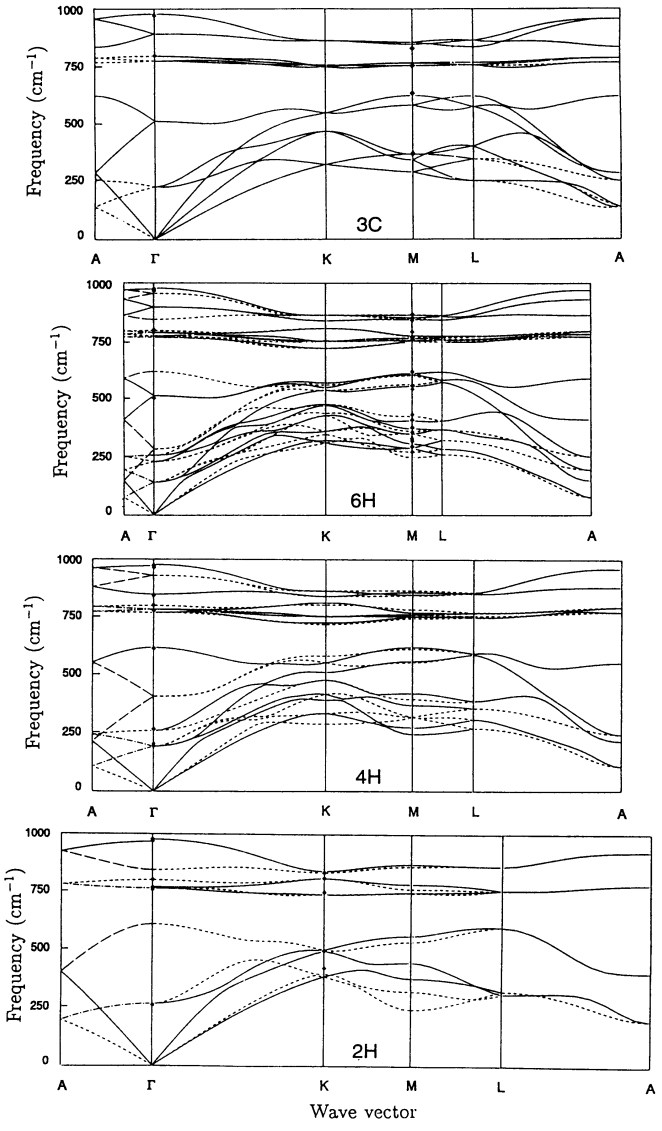

FIG. 4. Phonon dispersion curves for the $2H$-, $3C$-, $4H$-, and $6H$-SiC polytypes along high-symmetry lines in the hexagonal Brillouin zone. The experimental data from Tables I and II are represented by circles, triangles, and crosses. At the M point of the $6H$ structure additional experimental frequencies from Ref. 38 are also indicated. Solid, short-dashed, long-dashed, and dot-dashed lines indicate different polarization states. Their classification follows the transformation behavior of the phonon eigenvectors with the point-group operations.

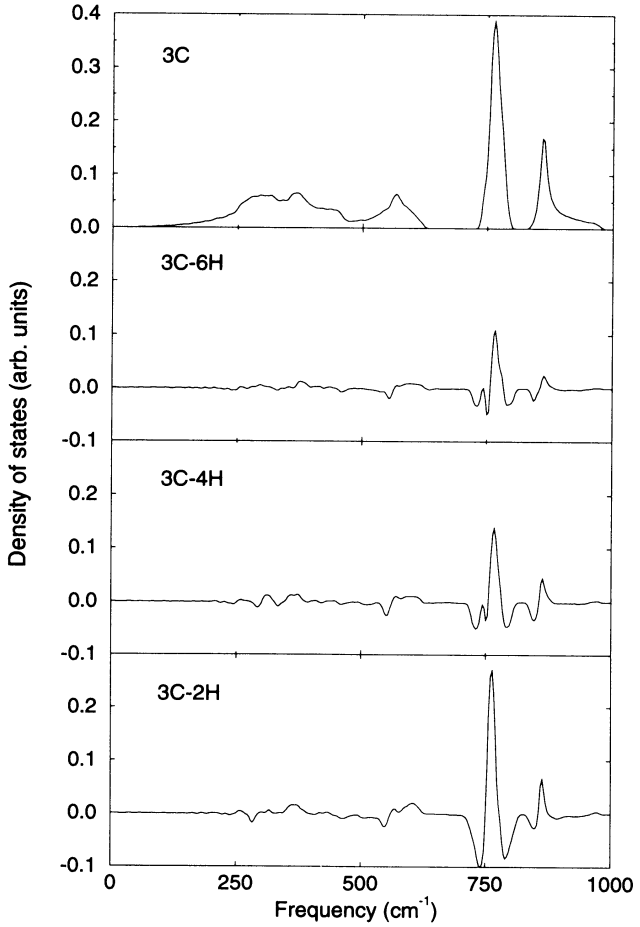

FIG. 5. Density of states of the four polytypes under consideration. Whereas the total one is plotted for $3C$-SiC (uppermost panel), only the deviations from this one are shown for the hexagonal structures $6H$, $4H$, and $2H$ (lower panels).

changes in the curvature, i.e., in the first derivatives of the phonon bands with respect to the wave vector, which modify the density of states.

C. Eigenvectors

In diamond and zinc-blende structure the eigenvectors of the different phonon modes with the branch index j and the wave vector $\mathbf{q}$ from the first Brillouin zone along the high-symmetry lines ΓX and ΓL can be represented by[29,46]

$$\mathbf{u}_j^1(\mathbf{q}) = \pm c_j(\mathbf{q})\mathbf{e}_j(\mathbf{q}), \tag{6}$$
$$\mathbf{u}_j^2(\mathbf{q}) = \left[1 - c_j^2(\mathbf{q})\right]^{\frac{1}{2}} \exp\left[i\Phi_j(\mathbf{q})\right]\mathbf{e}_j(\mathbf{q}).$$

In expression (6) $\kappa = 1, 2$ denotes the two atoms in the unit cell with displacements $\mathbf{u}_j^\kappa(\mathbf{q})$ and polarization vectors $\mathbf{e}_j(\mathbf{q})$ for longitudinal (j=LO, LA) and transverse (j=TO,TA) vibrations. The amplitude of the C atoms displacements is given by $c_j(\mathbf{q})$. The real phase $\Phi_j(\mathbf{q})$ of the C atoms vibrations with respect to that of the C atoms is chosen so that $\Phi_j(0) = 0$ holds for the Γ point. The plus (minus) sign indicates acoustic (optic) modes.

The results for the phase and the amplitude of cubic $3C$-SiC obtained within our BCM are represented in Fig. 6. They are compared with results of *ab initio* calculations within the density-functional perturbation theory.[9] An excellent agreement between both theories is observed. This is a strong indication for the reliability of the used BCM. An important argument for such a conclusion is the correct description of the behavior

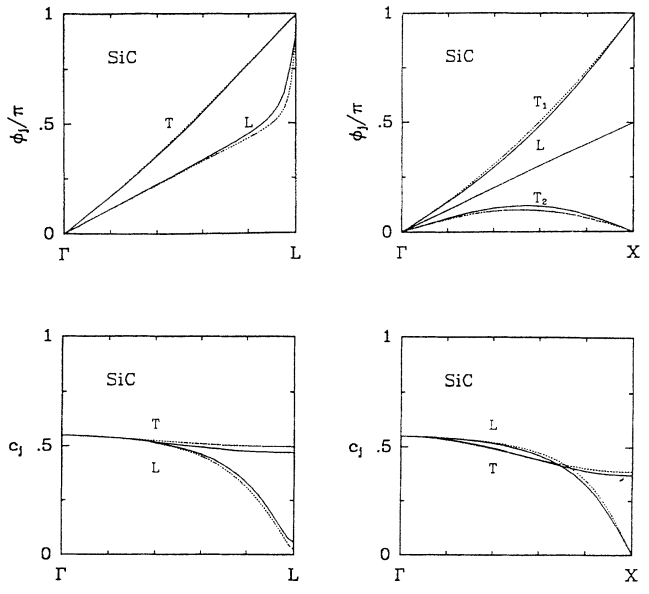

FIG. 6. Phase function $\Phi_j(\mathbf{q})$ (upper part) and amplitudes $c_j(\mathbf{q})$ (lower part) of carbon displacements [cf. Eqs. (6)] for $3C$-SiC along high-symmetry directions ΓL and ΓX in the Brillouin zone. Solid line, BCM; dotted line, *ab initio* calculations (Ref. 9).

of eigenvectors for longitudinal branches along the ΓL line. Their phase is particularly sensitive to the strength of the covalent bonding in the tetrahedrally coordinated semiconductors.[46] For instance, at the L point the longitudinal phase vanishes in the case of silicon,[29] whereas in diamond it is equal to π[46] leading to an opposite sign in the atomic displacements of the atoms in the unit cell.

We see again that the carbon atoms influence the physical properties of SiC much stronger than the silicon atoms. The eigenvectors of $3C$-SiC are similar to those of diamond. The phonon mode with $\Phi_l(L) = \pi$ is the bond-stretching mode. It causes a stretching of the bond in [111] direction, whereas the other three bond remain unchanged. On the other hand, the mode related to $\Phi_l(L) = 0$ possesses bond-bending character. It keeps the bond in [111] direction but gives rise to a change of the bond angles for the bonds in the other three directions.

From the knowledge of the phonon eigenvectors information about the internal-strain properties of the crystal can be extracted. The internal-strain tensor $\Delta_{\alpha\beta\gamma}(\kappa)$ is defined as the proportionality constant between the sublattice displacement $d_\alpha(\kappa)$ and the applied macroscopic strain $\varepsilon_{\beta\gamma}$ $(\alpha, \beta, \gamma = x, y, z)$ as

$$d_\alpha(\kappa) = -\sum_{\beta,\gamma} \Delta_{\alpha\beta\gamma}(\kappa)\varepsilon_{\beta\gamma}. \tag{7}$$

Symmetry requires that the tensors $\mathbf{\Delta}(\kappa)$ have only one independent component for diamond and zinc-blende materials,

$$\Delta_{\alpha\beta\gamma}(1) = -\Delta_{\alpha\beta\gamma}(2) = -\xi\frac{a_o}{4}\left|\epsilon_{\alpha\beta\gamma}\right|, \tag{8}$$

where ξ is the internal-strain parameter and $\epsilon_{\alpha\beta\gamma}$ is the fully antisymmetric Levi-Civita tensor.[47] The internal-strain parameter can be obtained from the longitudinal phase function $\Phi_l(\mathbf{q})$ for $\mathbf{q} = \frac{2\pi}{a}(\eta, \eta, \eta)$ and $\eta \to 0$ according to[29,48]

$$\xi = \frac{3}{2} - \frac{1}{\pi}\frac{\partial\Phi_l(\eta)}{\partial\eta}\bigg|_{\eta=0}. \tag{9}$$

From the results obtained for the phase function $\Phi_l(\mathbf{q})$ we derive a value $\xi = 0.36$. This value is in good agreement with the *ab initio* pseudopotential calculations[9] and approaches the average value of the experimental data for diamond $\xi = 0.125$ (Ref. 49) and silicon $\xi = 0.540$.[50] It is however smaller than the internal strain parameter derived from full-potential linear muffin-tin orbital (LMTO) calculations.[51]

D. Relations to elastic constants

From the dispersion curves of the acoustic phonons given in Figs. 3 and 4 the sound velocities for a propagation in the different space directions can be derived. These sound velocities are directly related to the independent elastic constants of the crystals. In the cubic case we have C_{11}, C_{12}, and C_{44}, whereas c_{11}, c_{33}, c_{13},

TABLE IV. Sound velocities for different propagation (first) and polarization (second) directions (in km/s).

Polytype	Propagation and polarization direction				
	xy	xz	xx	zz	xz (quasilong.)
$2H$	6.87	6.66	12.32	13.27	12.18
$4H$	6.94	6.65	12.42	13.41	12.36
$6H$	6.97	6.62	12.45	13.29	12.43
$3C$	8.21	5.64	12.81	13.29	12.70

c_{44}, and c_{66} are the independent elements of the tensor of elasticity moduli for hexagonal crystals.

The relation of these constants to the sound velocities are given not only for zinc-blende but also for hexagonal crystals in the Appendix of Ref. 52 ignoring the piezoelectric effect. In the hexagonal materials the characteristic Christoffel equations factorize, when the phonon propagation vector lies in the xy plane, that is normal to the z axis. The dispersion relation is independent of the propagation direction in this plane. There is one pure shear mode, propagating parallel to the x axis, polarized normal to the z axis ($\|$ y axis), and related to c_{66}, another pure shear mode, propagating parallel to the x axis, polarized parallel to the z axis, and related to c_{44}, and a pure longitudinal mode, propagating and polarized parallel to the x axis and related to c_{11}. For the phonon propagation in the meridian plane containing the z axis one has a pure longitudinal mode, propagating and polarized parallel to the z axis and related to c_{33}, as well as a quasilongitudinal one. We choose the mode with the strongest longitudinal character and propagating within the xz plane under an angle of 45° with the z axis. Its sound velocity is related to the elastic moduli c_{11}, c_{33}, c_{44}, and c_{13}, which allows the determination of c_{13}. The corresponding sound velocities derived from our BCM are listed in Table IV. Apart from that for the zz acoustic vibration in $4H$ they exhibit clear trends with respect to the hexagonality. It is not astonishing that the changes from $6H$ to $3C$ are larger than the variations within the hexagonal polytypes. This is related to the fact that $3C$ is not hexagonal in reality. Consequently the $3C$ modes have another symmetry. Therefore, in calculating the independent elastic stiffness constants C_{11}, C_{12}, and C_{44} we use the sound velocities along the [110] direction in the cubic material, v_l = 12.82 km/s and v_t = 8.17 and 5.56 km/s. The values in Table IV are in good agreement with the estimated ones made by Feldman *et al.*[18] (measurements by Arlt and Schodder[53] for a Lely-grown single $6H$-SiC crystal and Schreiber and Soga[54] for porous samples) of 7.53 (7.25, 7.69) km/s or 12.81 (13.26, 12.21) km/s for sound velocities in the planar and axial directions for the SiC polytypes. However, there seems to be an underestimation of the velocities of the TA-like modes by our theory.

The elastic moduli obtained for $3C$-, $6H$, $4H$-, and $2H$-SiC are listed in Table IV. In addition to the independent constants c_{11}, c_{33}, c_{44}, c_{66}, and c_{13} the elastic modulus c_{12} is estimated from the relation $c_{66} = \frac{1}{2}(c_{11} - c_{12})$.[52] However, the accuracy of this constant is low since it is remarkably influenced by the errors of both c_{11} and $2c_{66}$ in forming the difference $(c_{11} - 2c_{66})$. The moduli for $3C$ are recalculated from c_{11}, c_{12}, and c_{44} as described below. In principle we observe clear trends of the independent moduli versus hexagonality within the hexagonal polytypes. c_{11}, c_{66}, and c_{13} increase with decreasing hexagonality h, and c_{33} remains practically constant, whereas c_{44} slightly decreases with h. The values of the elastic constants for $6H$ and $4H$ are almost the same. This is in agreement with the findings of Helbig, Karmann, and Stein[55] that the two structures are very close to each other.

A complete and critical overview concerning the experimental studies of elastic constant of SiC is given in Ref. 51. In Table V we compare our results with more complete sets of elastic constants for hexagonal systems.[51,53,56] Arlt and Schodder[53] measured the complete set of elastic constants except for c_{13} of Lely-grown single $6H$-SiC by two different electroacoustical methods. Theoretical data are available from semiempirical calculations of Tolpygo[56] and LMTO studies of Lambrecht *et al.*[51] Whereas the results of Lambrecht *et al.*[51] are based on a first-principle method, Tolpygo[56] calculated the elastic constants for the $3C$ phase on the basis of a force model with parameters interpolated between those of silicon and diamond. The $3C$ results have been transformed to the hexagonal case in Ref. 51. The overall agreement of our results for four different polytypes and c_{ii} (i=1,3,4,6) with the experimental data for $6H$ as well as the values obtained theoretically is satisfying. The agreement with the LMTO calculation is poorer. This theory gives rise to too large moduli. On the other hand, the BCM overestimates the stiffness constants c_{13} and c_{12} remarkably. This results from the limited accuracy of

TABLE V. Elastic constants of hexagonal SiC polytypes (in Mbar) derived from sound velocities. For comparison values measured for $6H$ (Ref. 53) as well as calculated semiempirically (Ref. 56) or by LMTO (Ref. 51) for $3C$ and recalculated for hexagonal structures are also given.

Polytype	c_{11}	c_{33}	c_{44}	c_{66}	c_{13}	c_{12}
$2H$	4.87	5.65	1.42	1.52	1.39	1.83
$4H$	4.95	5.77	1.42	1.54	1.59	1.87
$6H$	4.98	5.67	1.41	1.56	1.76	1.86
$3C$	5.07	5.67	1.38	1.55	1.38	1.97
Ref. 53	5.02±0.20	5.65±0.11	1.69±0.03	2.03±0.06	–	0.95±0.29
Ref. 56	4.79	5.21	1.48	1.91	0.56	0.98
Ref. 51	5.60	6.07	1.94	2.40	0.33	0.79

TABLE VI. Elastic moduli C_{11}, C_{12}, and C_{44} for cubic $3C$-SiC (in Mbar) from present BCM, *ab initio* calculations of Lambrecht *et al.* (L) (Ref. 51) and Karch *et al.* (K), (Ref. 9) and force-constant models of Tolpygo (T) (Ref. 56) and Lee and Joannopoulos (LJ) (Ref. 15). The experimental data are recalculated from sound velocities of Feldmann *et al.* (Ref. 18) by Lambrecht *et al.* (Ref. 51).

Modulus	BCM	L	K	T	LJ	Expt.
C_{11}	4.13	4.20	3.90	3.52	3.71	3.90
C_{12}	2.14	1.26	1.36	1.40	1.69	1.42
C_{44}	2.15	2.87	2.53	2.33	1.76	2.56

their determination from sound relocities and the formulas from Ref. 52. As a consequence also the bulk moduli B are overestimated in comparison with the experimental value B=2.25 Mbar,[57] which is rather insensitive to the polytype.[39]

In the case of the zinc-blende $3C$-SiC more data, at least computed ones, exist. However, the elastic coefficients C_{11}, C_{12}, and C_{44} of the cubic system cannot be simply compared with those c_{ij} $(i,j = 1,...,6)$ of the hexagonal structures since the Cartesian coordinate systems are different. For instance, the z axis of the hexagonal lattice, which is parallel to the direction [0001], is the same as the [111] direction of cubic SiC. That means, the two different types of elastic stiffness constants for $3C$-SiC represented in the normal cubic Bravais lattice or the hexagonal system as in Table V can be related to each other by transformation matrices between the two Cartesian systems. Taking into account the independence of the volume compressibility, the linear compressibility, and the Young's modulus from the choice of the coordinate system as well as equality of sound velocities in the same direction one derives[58–60]

$$\begin{aligned} c_{11}+c_{12} &= 2(C_{11}+2C_{12}+C_{44})/3, \\ c_{11}-c_{12} &= 3(C_{11}-C_{12})C_{44}/(C_{11}-C_{12}+C_{44}), \\ c_{13} &= (C_{11}+2C_{12}-2C_{44})/3, \\ c_{33} &= (C_{11}+2C_{12}+4C_{44})/3, \\ c_{44} &= (C_{11}-C_{12}+C_{44})/3. \end{aligned} \tag{10}$$

Such transformation formulas are used for rewriting the $3C$ results presented in Table V. They are in agreement with the different definitions of the bulk modulus $B = (C_{11}+2C_{12})/3$ and $B = [c_{33}(c_{11}+c_{12})-2(c_{13})^2]/(c_{11}+c_{12}+2c_{33}-4c_{13})$.

For the cubic case the elastic constants calculated within the BCM are listed in Table VI. They are compared with other theoretical data[9,15,51,56] and moduli derived from sound velocities, which are extracted from Raman data for various polytypes[18] according to Ref. 51. We find a reasonable agreement with the experimental data and first principles results. This holds especially for C_{11}. However, the modulus C_{12} is overestimated. This is the main reason for the overestimation of the bulk modulus.

IV. SUMMARY

In the present paper we have applied the adiabatic bond-charge model to different SiC polytypes: the cubic $3C$ and the hexagonal $6H$, $4H$, and $2H$. The short-range elastic forces are described by two-body and three-body interactions between silicon ions, carbon ions, and bond charges. The long-range Coulomb forces are taken into account via an Ewald technique. The anisotropy of the system is described by differing forces and bond charges, according to the orientation of the underlying bonds with respect to the c axis. The parameters of the model are fit to frequencies derived from Raman and luminescence measurements. They show clear trends with the hexagonality of the polytypes.

The resulting phonon band structures along high-symmetry lines in the fcc and hexagonal Brillouin zone represent the experimental well-known features of the dispersion relations. This holds especially for the folding of the bands in [111] direction, when the number of Si-C bilayers is increased, the angular dispersion and the frequency splittings in the zone center. The anisotropy of the system is correctly described. It is essentially traced back to the macroscopy electric field related to the vibrating ions and bond charges. As a particularly sensitive test we show in the $3C$ case that the model calculations yields the same eigenvectors as *ab initio* calculations. From the resulting sound velocities we also derive the independent elastic constants of the different polytypes. They are in a reasonable agreement with those from measurements and other calculations. Discrepancies result from the fact that the sound velocities are not used as fit parameters in our model calculations.

ACKNOWLEDGMENTS

The authors are grateful to Professor D. Strauch for helpful discussions. This work has been supported by the Deutsche Forschungsgemeinschaft (Sonderforschungsbereich 196, project A8).

[1] A.R. Verma and P. Krishna, *Polymorphism and Polytypism in Crystals* (Wiley, New York, 1966).
[2] G.C. Trigunayat and G.K. Chada, Phys. Status Solidi A **4**, 9 (1971).
[3] N.W. Jepps and T.F. Page, Prog. Cryst. Growth Charact. **7**, 259 (1984).
[4] B. Winkler, M.T. Dove, E.K.H. Salje, M. Leslie, and B. Palosz, J. Phys. Condens. Matter **3**, 539 (1991).

[5] C. Cheng, V. Heine, and I.L. Jones, J. Phys. Condens. Matter **2**, 5097 (1990).
[6] N. Churcher, K. Kunc, and V. Heine, in *Proceedings of the 2nd International Conference on Phonon Physics*, Budapest, 1985, edited by J. Kollar, N. Kroo, N. Menyhard, and T. Siklos (World Scientific, Singapore, 1985), p. 956.
[7] C. Cheng, K. Kunc, and V. Heine, Phys. Rev. B **39**, 5892 (1989).
[8] W. Windl, K. Karch, P. Pavone, D. Schütt, D. Strauch, W.H. Weber, K.C. Hass, and L. Rimai, Phys. Rev. B **48**, 3164 (1993).
[9] K. Karch, Ph.D. thesis, Universität Regensburg, 1993; K. Karch, P. Pavone, W. Windl, O Schütt, and D. Strauch, (unpublished).
[10] B.H. Cheong, K.J. Chang, and M.L. Cohen, Phys. Rev. B **44**, 1053 (1991).
[11] J.F. Vetelino and S.S. Mitra, Phys. Rev. **178**, 1349 (1969).
[12] C.H. Hodges, Phys. Rev. **187**, 994 (1969).
[13] R. Banerjee and Y.P. Varshni, J. Phys. Soc. Jpn. **30**, 3015 (1971).
[14] T.N. Singh, G. Singh, and S.S. Kushwaha, Solid State Commun. **13**, 1393 (1973).
[15] D.H. Lee and J.D. Joannopoulos, Phys. Rev. Lett. **48**, 1846 (1982).
[16] M.S. Kushwaha, Phys. Status Solidi B **111**, 337 (1982).
[17] S.-I. Nakashima, Y. Nakakura, A. Wada, and K. Kunc, J. Phys. Soc. Jpn. **57**, 3828 (1988).
[18] D.W. Feldmann, J. Parker, W.J. Choyke, and L. Patrick, Phys. Rev. **170**, 698 (1968); **173**, 787 (1968).
[19] D. Olego and M. Cardona, Phys. Rev. B 25, 1151 (1982); D. Olego, M. Cardona, and P. Vogl, *ibid.* **25**, 3878 (1982).
[20] S.-I. Nakashima, A. Wada, and Z. Inoue, J. Phys. Soc. Jpn. **56**, 3375 (1987).
[21] L. Patrick, Phys. Rev. **167**, 809 (1968).
[22] G.B. Dubrowskii and A.A. Lepneva, Fiz. Tverd. Tela **21**, 1930 (1979) [Sov. Phys. Solid State **21**, 1110 (1979)]; **25**, 2317 (1983) [**25**, 1330 (1983)].
[23] F. Engelbrecht and R. Helbig, Phys. Rev. B **48**, 15698 (1993).
[24] H. Hobert and H. Dunken (unpublished).
[25] L. Patrick, D.R. Hamilton, and W.J. Choyke, Phys. Rev. **143**, 526 (1966).
[26] R.G. Humphreys, D. Bimberg, and W.J. Choyke, Solid State Commun. **39**, 163 (1981).
[27] W. Weber, Phys. Rev. B **15**, 4789 (1977); K. C. Rustagi and W. Weber, Solid State Commun. **18**, 673 (1976).
[28] R.S. Leigh, B. Szigeti, and V.K. Tewary, Proc. R. Soc. London A **320**, 505 (1971).
[29] D. Strauch, A.P. Mayer, and B. Dorner, Z. Phys. B **78**, 504 (1990).
[30] R. Turbino, L. Piseri, and G. Zubi, J. Chem. Phys. **56**, 1022 (1972).
[31] C. Falter, W. Ludwig, and M. Selmke, Solid State Commun. **54**, 497 (1985).
[32] J.C. Phillips, Phys. Rev. **166**, 832 (1968).
[33] R.M. Martin, Phys. Rev. **186**, 871 (1969).
[34] P.J.H. Denteneer and W. van Haeringen, Phys. Rev. B **33**, 2831 (1986).
[35] L. Miglio and C. Colombo, Surf. Sci. **221**, 486 (1989).
[36] A. Garcia and M.L. Cohen, Phys. Rev. B **47**, 4221 (1993).
[37] P.P. Ewald, Ann. Phys. (Leipzig) **64**, 253 (1921).
[38] *Numerical Data and Functional Relationships in Science and Technology*, edited by O. Madelung, Landolt-Börnstein, New Series, Group III, Vol. 17a (1982) and Vol. 22a (1986) (Springer, Berlin).
[39] P. Käckell, B. Wenzien, and F. Bechstedt, Phys. Rev. B (to be published).
[40] P.N. Keating, Phys. Rev. **145**, 637 (1966).
[41] O.H. Nielsen and W. Weber, Comput. Phys. Commun. **18**, 101 (1979).
[42] G. Echold, M. Stein-Arsic, and H.J. Weber, J. Appl. Crystallogr. **20**, 134 (1987).
[43] K. Karch, diploma thesis, Universität Regensburg, 1990; D. Strauch, B. Dorner, and K. Karch, in *Proceedings of the Third International Conference on Phonon Physics*, Heidelberg, 1989, edited by S. Hunklinger, W. Ludwig, and G. Weisser (World Scientific, Singapore, 1990), p. 82.
[44] H. Wendel and R.M. Martin, Phys. Rev. B **19**, 5251 (1979).
[45] R. Loudon, Adv. Phys. **13**, 423 (1963).
[46] P. Pavone, K. Karch, O. Schütt, W. Windl, D. Strauch, P. Gianozzi, and S. Baroni, Phys. Rev. B **48**, 3156 (1993).
[47] L. Kleinman, Phys. Rev. **128**, 2614 (1962).
[48] P. Pavone, Ph.D. thesis, Scuola Internazionale Superiore di Studi Avanzati–International School for Advanced Studies, Trieste, 1991.
[49] C.S.G. Cousins, L. Gerward, J.S. Olsen, and B.J. Sheldon, J. Phys. Condens. Matter **1**, 4511 (1989).
[50] M. Cardona, K. Kunc, and R.M. Martin, Solid State Commun. **44**, 1205 (1982).
[51] W.R. Lambrecht, B. Segall, M. Methfessel, and M. van Schilfgaarde, Phys. Rev. B **44**, 3685 (1991).
[52] B.A. Auld, *Acoustic Fields and Waves in Solids* (R.E. Krieger, Malabar, FL, 1990), Vol. I.
[53] G. Arlt and G.R. Schodder, J. Acoust. Soc. Am. **370**, 384 (1965).
[54] E. Schreiber and N. Soga, J. Am. Ceram. Soc. **49**, 342 (1966).
[55] R. Helbig, S. Karmann, and R.A. Stein, *Extended Abstracts of the Electrochemical Society* (Electrochemical Society, Hollywood, FL, 1989), p. 718.
[56] K.B. Tolpygo, Fiz. Tverd. Tela (Leningrad) **2**, 2655 (1960) [Sov. Phys. Solid State **2**, 2367 (1960)].
[57] R.D. Carnahan, J. Am. Ceram. Soc. **51**, 223 (1968).
[58] J.F. Nye, *Physical Properties of Crystals* (Clarendon, Oxford, 1957), Chap. VIII.
[59] J.B. Wachtman and D.G. Lam, J. Am. Ceram. Soc. **42**, 254 (1959).
[60] B.P. Pandey and B. Dayal, Phys. Status Solidi B **58**, K53 (1973).